Evidence of antimagnetic rotational motion in math xmlns="http://www.w3.org/1998/Math/MathML">mmultiscripts>mi>Pd/mi>mprescripts>/mprescripts>none>/none>mn>103/mn>/mmultiscripts>/math>

A. Sharma, R. Raut, S. Muralithar, R. P. Singh, S. S. Bhattacharjee, S. Das, S. Samanta, S. S. Ghugre, R. Palit, S. Jehangir, N. Rather, G. H. Bhat, J. A. Sheikh, S. S. Tiwary, Neelam, P. V. Madhusudhana Rao, U. Garg, and S. K. Dhiman

Phys. Rev. C **103**, 024324 — Published 25 February 2021

DOI: 10.1103/PhysRevC.103.024324

Evidence of antimagnetic rotational motion in ^{103}Pd

A. Sharma,[1,*] R. Raut,[2] S. Muralithar,[3] R. P. Singh,[3,†] S. S. Bhattacharjee,[3] S. Das,[2] S. Samanta,[2] S. S. Ghugre,[2] R. Palit,[4] S. Jehangir,[4] N. Rather,[5] G.H. Bhat,[6] J.A. Sheikh,[7] S. S. Tiwary,[8] Neelam,[9] P. V. Madhusudhana Rao,[10] U. Garg,[11] and S. K. Dhiman[1]

[1]*Department of Physics, Himachal Pradesh University, Shimla - 171005, India*
[2]*UGC-DAE Consortium for Scientific Research, Kolkata Centre, Kolkata - 700098, India*
[3]*Nuclear Physics Group, Inter-University Accelerator Centre, New Delhi - 110067, India*
[4]*Department of Nuclear and Atomic Physics, Tata Institute of Fundamental Research, Mumbai - 400005, India*
[5]*Department of Physics, Islamic University of Science and Technology, Awantipora, Jammu and Kashmir - 192122, India*
[6]*Department of Physics, SP College Srinagar, Jammu and Kashmir, 190001, India*
[7]*Department of Physics, University of Kashmir, Srinagar, 190006, India*
[8]*Department of Physics, Institute of Science, Banaras Hindu University, Varanasi - 221005, India*
[9]*Department of Physics and Astrophysics, University of Delhi, New Delhi - 110007, India*
[10]*Department of Nuclear Physics, Andhra University, Visakhapatnam - 530003, India*
[11]*Department of Physics, University of Notre Dame, Notre Dame, Indiana - 46556, USA*

Lifetime measurements have been carried out for the levels of the negative parity yrast sequence in ^{103}Pd nucleus using the Doppler shift attenuation method (DSAM). The levels were populated via ^{94}Zr(^{13}C, 4nγ)^{103}Pd fusion-evaporation reaction at a beam energy of 55 MeV. De-exciting γ rays were detected by utilizing the Indian National Gamma Array (INGA). The extracted transition probabilities and other auxiliary observations indicate that the sequence may be resulting from the antimagnetic rotational (AMR) motion of valence nucleons. The key characteristic feature of the AMR motion is the steady decrease of the $B(E2)$ transition probability with spin, which is seen in the present measured transitions for ^{103}Pd. The experimental results are compared with the theoretical predictions of tilted axis cranked approach based on the covariant density functional theory (TAC-CDFT). It is noted that the properties of the AMR band structure for ^{103}Pd predicted in this model analysis are in good agreement with the present experimental findings. Further, semi-classical particle-rotor model (SCM) has been employed to substantiate the AMR interpretation of the observed band structure in ^{103}Pd and it is shown that results are similar to the band structures observed in the neighboring isotopes, which have also been considered as candidates for AMR motion.

I. INTRODUCTION

Most of the nuclei are known to exhibit rotational spectra similar to that observed in molecules with energy roughly proportional to square of the angular-momentum. Quadrupole deformation of nucleus leads to these rotational bands with strong $E2$ transitions between the states. The bands are well understood as a collective rotation of many nucleons around an axis perpendicular to the symmetry axis of the deformed density distribution [1]. Such band structures have been well investigated, both experimentally and theoretically, for many decades now. It has been recently observed that valance nucleons occupying high-j orbitals around doubly magic core may result into a new kind of structural phenomena such as the magnetic rotation (MR) and the antimagnetic rotation (AMR) [2–5]. These are sequences of transitions bearing tentative similarity with rotational bands, but are observed in nuclei around the shell closures and typically with small deformation. In an MR band, the total angular momentum is generated by the coupling of proton and neutron angular momentum vectors oriented almost perpendicular to each other at the band head. The angular momentum along the band is generated by the alignment of the two spin vectors along the rotational axis in a way that resembles closing the blades of a pair of shears, thus also rendering the name shears band to such sequences. The MR bands can be differentiated from the conventional rotational bands by the cascade of strong $M1$ intra-band transitions and weak crossover $E2$ transitions. The AMR bands are understood in terms of a twin shears mechanism, wherein the angular momentum is generated by the simultaneous closing of the two (or more) symmetric and anti-aligned proton-hole blades onto the neutron-particle angular momentum vectors [5]. The anti-alignment of the two (or more) proton-hole blades cancel the perpendicular component of each others magnetic moment leading to the absence of magnetic dipole transitions. This cancellation of dipole moments is akin to anti-ferromagnetism and the name AMR has been assigned to such bands. The characteristic features of the AMR band include weak intra-band $E2$ transitions and decreasing transition probability ($B(E2)$) values with increasing spin. The dynamic moment of inertia to reduced transition probability ratio ($\Im^{(2)}/B(E2)$) assume large values, that increase with spin, and may exceed 100 $\hbar^2\text{MeV}^{-1}(eb)^{-2}$. Similar val-

* anupriya.jotu@gmail.com
† rajeshpratap07@gmail.com

ues of $\Im^{(2)}/B(E2)$ are also observed for super-deformed bands, albeit with much larger quadrupole deformations than those typically underlying the AMR sequences. The aforesaid variation of transition probabilities within the MR and the AMR sequences are known to be one of their distinguishing signature of such structures. Consequently, lifetime measurement of the levels in these bands, where from the transition probabilities can be extracted, are of paramount significance in their ascription.

Nuclei in the A≈110 region, near the Z≈50 shell closure, with the $h_{11/2}$ neutron particles and the $g_{9/2}$ proton holes are suitable candidates for observation of the twin shears mechanism. Indeed, AMR bands have been reported in a number of nuclei in this region such as $^{105-110}$Cd [6–12] and ^{100,101,104}Pd [13–17]. The present paper reports lifetime measurement of some of the levels constituting the negative parity yrast band in ^{103}Pd (Z=46, N=57) (FIG. 1) and interpretation of the sequence as one resulting from the AMR phenomenon. The sequence was previously established from measurements by Jerrestam *et al.* [18] and Nyako *et al.* [19]. The latter had interpreted the band to be α= -1/2 signature branch of $\pi(g_{9/2})^{-4} \otimes \nu h_{11/2}(g_{7/2}, d_{5/2})^6$ configuration. Recent theoretical calculations in the framework of tilted axis cranking model based on the covariant density functional theory (TAC-CDFT) have predicted the sequence to be stemming from the AMR mechanism based on $\pi(g_{9/2})^{-4} \otimes \nu h_{11/2}(g_{7/2}, d_{5/2})^6$ configuration [20]. It has been proposed that these bands in Pd isotopes are generated from the closing of four proton-hole blades towards the neutron-particle angular momentum vectors [21]. This resembles the closing of an umbrella (Fig. 4 of Ref.[20]) and the corresponding phenomenon has been called as "umbrella-like antimagnetic rotation (UAMR)". The interpretation has been largely validated with respect to the analogous sequences observed in the neighboring ^{101,104}Pd isotopes [20], wherein lifetime measurements exist [14–16] (that have been used by Jia *et. al* [20]). The behavior of $B(E2)$ and $\Im^{(2)}/B(E2)$ in these isotopes could be reproduced well in the TAC-CDFT calculations. An investigation to extend the confirmation of the novel UAMR mode of excitation to other Pd isotope is warranted and has been addressed in this paper for ^{103}Pd.

The characteristic properties of MR and AMR bands have also been successfully studied with the help of semi-classical particle rotor model (SCM) in many nuclei [6–16]. This is essentially a geometric model that assumes a shears like structure of the high-j proton-holes and neutron particles that close to generate the high spin states [3, 22]. It is shown in the present work that the experimental observables of ^{103}Pd viz. the level energies and the $B(E2)$ values are successfully reproduced using this model, thus providing a further evidence that the negative parity yrast sequence of ^{103}Pd arises from the AMR motion.

II. EXPERIMENTAL DETAILS

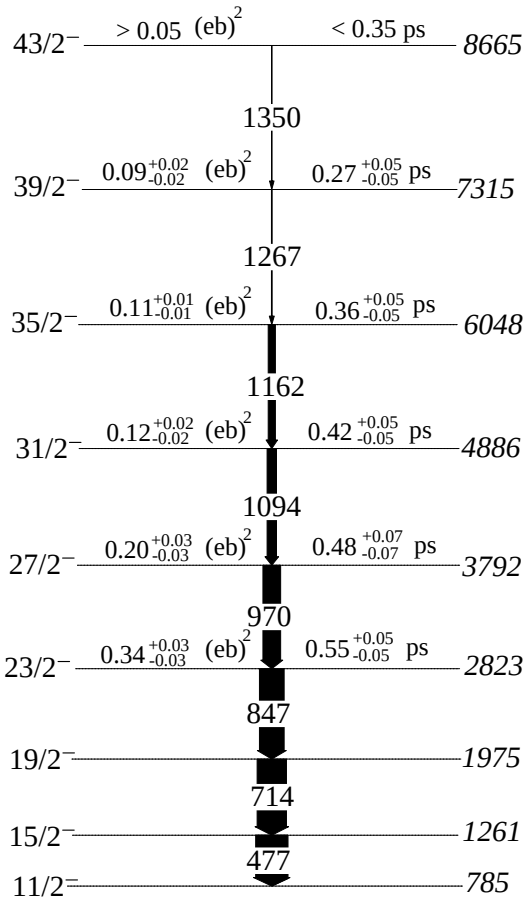

FIG. 1. The $\nu h_{11/2}$ band in ^{103}Pd, as reported in Ref. [19]. The values of lifetime and the transition probability mentioned for the states are from the present work.

High spin states of ^{103}Pd were populated using ^{94}Zr(^{13}C, 4n)^{103}Pd fusion-evaporation reaction. The ^{13}C beam at E_{lab} 55 MeV was provided by 15 UD pelletron accelerator at the Inter University Accelerator Centre (IUAC) [23], New Delhi. The beam was impinged on a 1 mg/cm^2 thick ^{94}Zr target, evaporated on a 10 mg/cm^2 thick gold. The de-exciting γ-rays were detected using eighteen Compton suppressed HPGe clover detectors constituting the Indian National Gamma Array (INGA) [24] setup at IUAC. The clover detectors were mounted at 5 different angles with respect to the beam axis, *viz*, two at θ = 32° (ϕ = 0°, 180°), two at 57° (ϕ = 135°, 315°), six at 90° (ϕ = 0°, 45°, 135°, 180°, 225°, 315°), four at 123° (ϕ = 45°, 135°, 225°, 315°) and four at 148° (ϕ = 0°, 90°, 180°, 270°). A total of about 2.5× 10^9 two and higher fold coincidence events were recorded using

a CAMAC-based data acquisition system [25]. The acquired list mode data were sorted into symmetric as well as angle dependent asymmetric γ-γ matrices using INGASORT [26] code, for subsequent analysis.

III. DATA ANALYSIS

The γ-γ matrices were analyzed using the INGASORT [26] and RADWARE [27] software packages. The level scheme of the ^{103}Pd nucleus was observed up to an excitation energy 8.665 MeV and spin $43/2^-$. The analysis for determining the level lifetimes was carried out using the LINESHAPE package [28] along with the developments reported in Ref. [29]. The latter pertains to the simulation of velocity profiles of the residues traversing the target and the backing media with inputs of ion transport trajectories calculated using the TRIM [30] software and energy-angle distribution of the residues, following particle evaporation from the compound nucleus, using the statistical model codes such as PACE4 [31]. As per the conventional procedure of analysis in the DSAM, the velocity profile, along with other inputs (γ-ray energy, angle of observation, etc.), were used to calculate the Doppler shapes on the transitions of interest at different angles characterizing the detector setup. The calculated shapes were then least-square fitted to the experimental spectra in order to determine the level lifetimes. The parameters of fitting were the level lifetime, the respective side feeding time (if any) as well as spectral parameters such as the height of the transition peak of interest and any neighboring contaminant, and the spectrum background. In case of incorporating the side feeding contribution to the observed experimental γ-ray transition peak, the same was modeled with a single feeder state for each level of interest. The intensity of the feeding was determined from the analysis of the level scheme while the lifetime of the feeder state, that is the feeding time, was a parameter in the minimization process. To ensure the reliability of the present results, two different gating conditions, namely, 'gate on the transition above' (GTA) and 'gate on the transition below' (GTB) were employed. A rotational cascade of five levels with constant dynamic moment of inertia ($\Im^{(2)} \approx 40\ \hbar^2\ \mathrm{MeV}^{-1}$) was considered as the side-feeding. The dynamic moment of inertia is estimated by using the relation [32]:

$$\Im^{(2)}(I) = \frac{4\hbar^2}{E(I+2 \rightarrow I) - E(I \rightarrow I-2)}$$

The representative fits of the Doppler broadened lineshapes observed in the experimental spectra, under GTA and GTB, are illustrated in FIG. 2. The spectra for analysis were extracted from angle-dependent asymmetric matrices, each with the γ-ray observed at one of the five (148°, 123°, 90°, 57° and 32°) possible angles on the x-axis and coincident γ-rays detected in any of the other (four) angles on y-axis. The gate was applied on a transition recorded on the y-axis and projected on the x-axis, corresponding to a specific angle, of the respective matrix. The spectra corresponding to GTB was extracted with a gate on the 477 keV transition. The entire cascade of transitions, consisting of 847, 970, 1094, 1162, 1267 and 1350 keV γ-rays was analyzed therefrom. The chi-square minimization exercise was carried out simultaneously with experimental spectra at five different angles, that facilitated in constraining with fitting parameters. The procedure was pursued in two steps. In the first round, the level lifetime, the side feeding time and the spectral parameters were varied for each transition of the cascade, individually, starting from the top, in order to obtain the best-fitted values. The spectral parameters, such as peak height and the background, were then held fixed and the lifetimes and the side feeding times of the levels in the cascade were allowed to vary together (globally) for concluding on their final values. It is known that the side feeding process introduces an element of uncertainty on the result obtained from the DSAM, following which it is always of preference to carry out the analysis using experimental spectra generated with the GTA. The latter eliminates any feeding contribution to the transition peaks of interest but it is often plagued with lack of statistics for a reliable fitting. Analysis using GTA spectrum, is nevertheless been carried out in the present work, albeit only for some of transitions for which it is possible to pursue the procedure that has been detailed elsewhere [33]. The technique encompasses the inclusion of the feeding history of the state de-excited by the gating transition while analyzing for the lifetimes levels below. It is also noteworthy that the spectra with GTA were generated with separate gating transitions for analysis of different levels in the cascade. The level lifetimes of the 6048, 4886, and 3792 keV states were analyzed from 1267 keV gated spectra while that of the 2823 keV level was extracted from the 970 keV gated ones. The latter one was so chosen for lack of statistics on the Doppler broadened lineshape of 847 keV transition peak, de-exciting the 2823 keV state, when observed in the gate on the 1267 keV transition.

The uncertainties on the lifetime results include those extracted from chi-square analysis with respect to the level lifetime and, if applicable (GTB case), the side feeding time. The uncertainties on the lifetime values also include the systematic contributions from that of the stopping powers, which is known to be about 5% [30], when extracted from the updated and experimentally benchmarked SRIM software, as in the present case. The uncertainties on the stopping powers, determined thus, are rather small vis a vis the ones that result from using one of the previous models incorporated in the conventional LINESHAPE package. This curb on stopping uncertainties has been the merit of the current analysis.

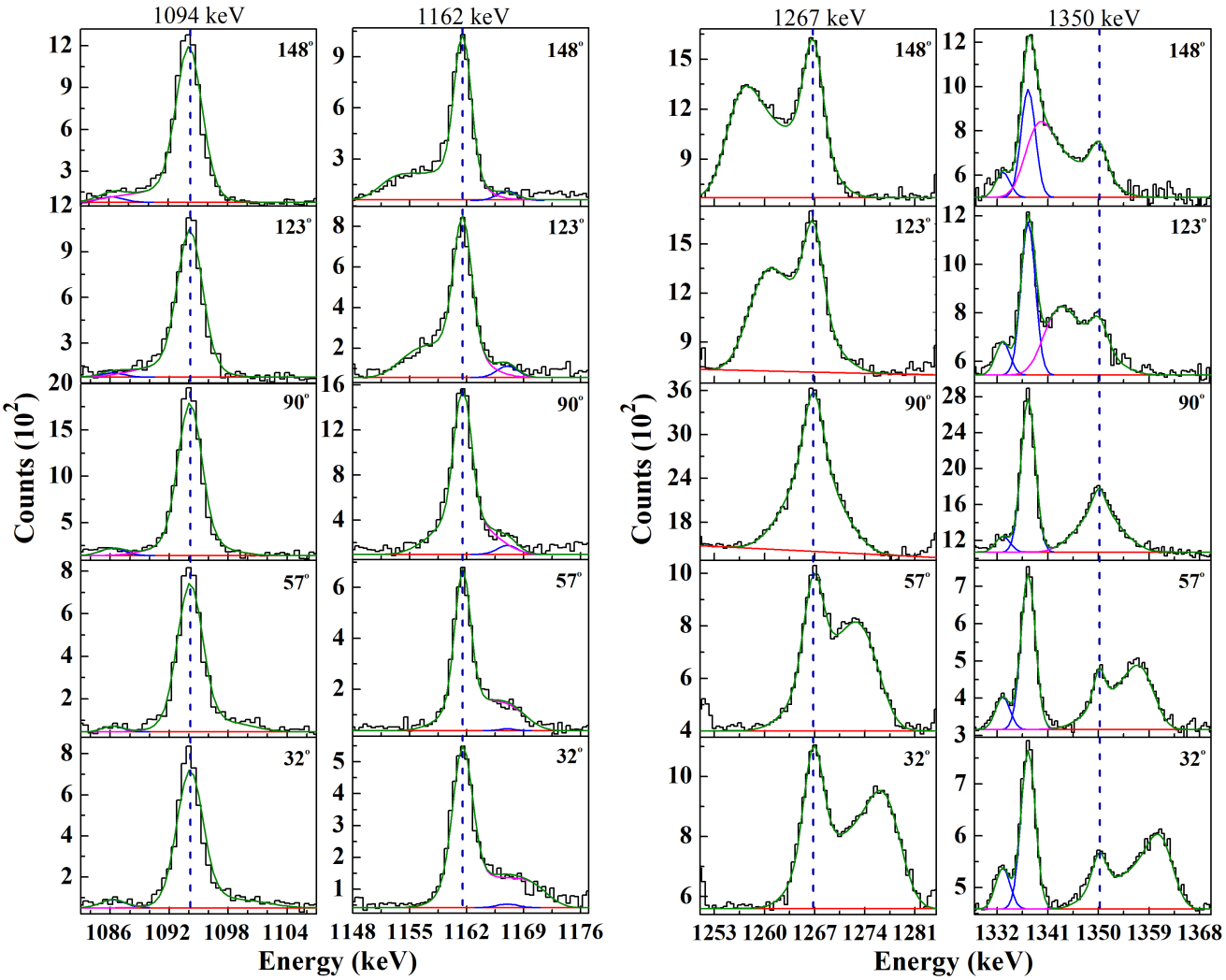

FIG. 2. Experimentally observed spectra along with the fitted lineshapes for the 1094 keV, 1162 keV, 1267 keV, and 1350 keV γ-rays in ^{103}Pd. The obtained lineshape of the γ rays, contaminant peaks, the total lineshapes and background are represented by the magenta, blue, green and red colors, respectively. The vertical dashed line represents the stopped peak position for each transition. Left: Spectra obtained from gate on 1267 keV transition (GTA). Right: Spectra obtained from gate on 477 keV transition (GTB).

IV. RESULTS

The level lifetimes in the negative parity yrast band of the ^{103}Pd nucleus, as determined from the present work, are recorded in Table 1. It is noteworthy that the lifetime of topmost level in the sequence, determined from GTB spectra, is only an upper limit on the same, as obtained from conventional analysis using the LINESHAPE code. The reduced transition probabilities has been calculated from extracted level lifetimes and the results are also presented in the table. The equation used for the purpose is

$$B(E2) = \frac{0.0816 f_\gamma(E2)}{E_\gamma^5(E2)[1+\alpha_t(E2)]\tau}[(eb)^2] \qquad (1)$$

where $\alpha_t(E2)$ is the total internal conversion coefficient of the transition and $f_\gamma(E2)$ is the branching ratio. Here $f_\gamma(E2)$= 1 since there is no other branch; and for $E_\gamma \geq$ 100 keV the total internal conversion coefficient of the transition $\alpha_t(E2)$ is assumed to be negligible. The lifetime inputs in the $B(E2)$ calculations are those obtained from analysis using the GTA, if available. In the absence of the latter as in the case of the $39/2^-$ and $43/2^-$ levels of the sequence, lifetimes extracted from analyzing the GTB spectra have been used. The significance of these experimental results in the context of the physics, that is aspired in this paper, is addressed in the next section.

TABLE I. Level lifetimes for the negative parity yrast band in ^{103}Pd as obtained in the present investigation using both GTA (gate on the transition above) and GTB (gate on the transition below) methods; $\tau_{\rm S.F.}$ are the side feeding lifetime values obtained from the GTB analysis. The reduced transition probabilities $B(E2)$ for the $39/2^-$ and the $43/2^-$ states were calculated from the respective $\tau_{\rm GTB}$ while those for the other states were calculated using $\tau_{\rm GTA}$

I^π ($\hbar$)	E_γ [MeV]	$\tau_{\rm GTA}$ (ps)	$\tau_{\rm GTB}$ (ps)	$\tau_{\rm S.F.}$ (ps)	$B(E2)\downarrow$ (eb)^2	$\Im^{(2)}/B(E2)$ $\hbar^2$MeV$^{-1}/(eb)^2$
$23/2^-$	0.847	$0.55^{+0.05}_{-0.05}$	$0.54^{+0.08}_{-0.06}$	$2.60^{+0.08}_{-0.06}$	$0.34^{+0.03}_{-0.03}$	95^{+9}_{-9}
$27/2^-$	0.970	$0.48^{+0.07}_{-0.07}$	$0.49^{+0.05}_{-0.05}$	$0.81^{+0.05}_{-0.05}$	$0.20^{+0.03}_{-0.03}$	161^{+22}_{-23}
$31/2^-$	1.094	$0.42^{+0.05}_{-0.05}$	$0.43^{+0.05}_{-0.05}$	$0.34^{+0.05}_{-0.05}$	$0.12^{+0.02}_{-0.02}$	495^{+63}_{-63}
$35/2^-$	1.162	$0.36^{+0.05}_{-0.05}$	$0.35^{+0.05}_{-0.05}$	$0.21^{+0.05}_{-0.05}$	$0.11^{+0.01}_{-0.01}$	358^{+50}_{-50}
$39/2^-$	1.267		$0.27^{+0.05}_{-0.05}$	$0.11^{+0.05}_{-0.05}$	$0.09^{+0.02}_{-0.02}$	524^{+101}_{-96}
$43/2^-$	1.350		<0.35		>0.05	<532

V. DISCUSSION

In this section, the experimental results shall be discussed in the frameworks of the Total Routhian Surface (TRS), TAC-CDFT and SCM approaches. The TRS calculations were done within cranked Hartree-Fock-Bogoliubov (CHFB) framework with Strutinsky's shell correction procedure. The potential used was of Woods-Saxon type with monopole pairing interaction [35, 36]. The values of pairing gap 'Δ' and chemical potential 'λ' were calculated by solving the BCS equations self-consistently at rotational frequency $\omega = 0$; for higher rotational frequencies Δ was assumed to vary smoothly as a function of ω such that at ω=ω_c, $\Delta = \Delta_o/2$, where Δ_o is the value of Δ at $\omega = 0$, following the prescription given in Ref. [37]. The value of ω_c was assumed to be 0.7 MeV for both, neutrons and protons (variations of ω_c from 0.7 to 0.9 MeV did not have any significant effect on the results). TRS calculations were done for the yrast band in the $\beta_2 - \gamma$ plane as a function of rotational frequency and for each mesh point the total energy was minimized with respect to hexadecapole deformation parameter β_4. The result for some rotational frequencies (ω) is provided in FIG. 3 for the yrast band. For $\hbar\omega = 0.4$ MeV, figure depicts shallow minimum with deformation parameters, $\beta_2 = 0.16$, $\gamma = 3°$, $\beta_4 = 0.016$. At higher rotational frequencies, the minimum moves towards the prolate axis with reduced deformation, at $\hbar\omega = 0.6$ MeV, β_2= 0.05. Similar results have been obtained by Ashley *et al.* for ^{103}Pd [38] and Zhang *et al.* [21] for ^{101}Pd. The $B(E2)$ values calculated from the predicted deformation in the frequency range of 0.4 to 0.65 MeV, varies from 0.12 to 0.01 $(eb)^2$. TRS results, thus significantly underpredict the experimentally determined $B(E2)$ values.

Recently, it has become feasible to apply the microscopic model of TAC-CDFT to investigate the MR and AMR band structures in atomic nuclei. In this model, angular-momentum is generated using the cranking approximation with the mean-field derived from the relativistic Dirac approach. This effective mean-field approach considers all the nucleons in the system to obtain the mean-field. However, in order to perform a configuration constrained calculations, it is important to choose a core and in Ref. [20] ^{100}Sn has been used as a closed core. In the case of Pd isotopes, the configuration assumed is $\pi(g_{9/2})^{-4} \otimes \nu(h_{11/2})^m(g_{7/2}, d_{5/2})^n$ with $(m = 1, 2; n = 4, 6)$ [20]. The rotational frequencies and $B(E2)$ values are compared with the TAC-CDFT predictions in Figs. 5 and 6. It is thus, noted that TAC-CDFT calculations reasonably reproduce the level energies and the decreasing trend of the $B(E2)$ along the sequence. The decrease in the $B(E2)$ with increasing spin is known to be a fingerprint of the AMR mechanism and thus supports that the negative parity yrast sequence in the ^{103}Pd nucleus

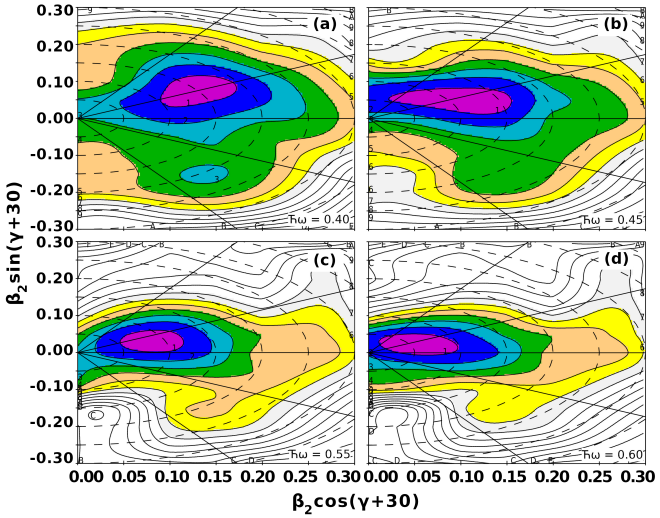

FIG. 3. Contour plots from TRS calculations for the negative parity yrast band in ^{103}Pd at rotational frequencies ($\hbar\omega$) = 0.40 MeV (a), 0.45 MeV (b), 0.55 MeV (c) and 0.60 MeV (d). The energy difference between two consecutive contours is 300 keV.

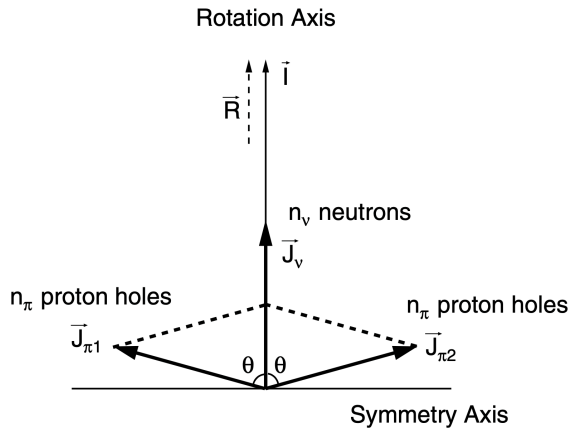

FIG. 4. Schematic diagram for angular momentum coupling of the proton-hole blades ($\vec{J}_{\pi_1}$ and $\vec{J}_{\pi_2}$), the neutron blade ($\vec{J}_\nu$) and the core rotation ($\vec{R}$) as discussed in the text. The figure is taken from Ref. [34]

.

may originate from the AMR motion. The general agreement of the experimental level energies and $B(E2)$ values with the predictions of the TAC-CDFT, as reported by Jia *et al.* [20], favors the configuration assignment of $\pi(g_{9/2})^{-4} \otimes \nu h_{11/2}(g_{7/2}, d_{5/2})^6$ for the observed band in ^{103}Pd. It is noted that TAC-CDFT constrained solution for this configuration was obtained only in the rotational frequency range of $\hbar\omega = 0.36 - 0.64$ MeV. The observed states, below and above this frequency range, may have different intrinsic configurations.

To further substantiate the AMR interpretation of the observed band structure in ^{103}Pd, we have also performed SCM analysis as has been carried out for the neighboring isotopes [14, 34]. In this model, the n_π number of high-j proton-holes that are deformation aligned and the n_ν number of high-j neutron-particles that are rotation aligned are represented by classical angular momentum vectors (blades). The model is schematically shown in FIG. 4. The total energy of the system is the sum of the energy from core rotation and the effective interaction of the type $V_2 P_2(\theta)$ that is assumed between the blades [14]. The total angular momentum $\vec{I}$ is the sum of the angular momenta from the proton-hole blades $\vec{J}_{\pi_1}$, $\vec{J}_{\pi_2}$, the neutron blade $\vec{J}_\nu$ and the rotation $\vec{R}$ of the core. It is assumed that each of the two blades $\vec{J}_{\pi_1}$ and $\vec{J}_{\pi_2}$ consist of n_π proton holes with mutually aligned angular momenta. The neutron blade $\vec{J}_\nu$ results from n_ν neutrons, all with rotation aligned angular momenta. The angle (θ) between the proton-hole blade and the neutron blade is the dynamical variable. The energy expression for the system in the units of $\hbar$ is given by [34]

$$E(I,\theta) = \frac{(\vec{I} - \vec{J}_{\pi_1} - \vec{J}_{\pi_2} - \vec{J}_\nu)^2}{2I_m} + 2V_0 n_\pi n_\nu \times \left(\frac{3\cos^2\theta - 1}{2}\right) - V_0 n_\pi^2 \left(\frac{3\cos^2 2\theta - 3}{2}\right) + I\omega_0 \quad (2)$$

where I_m stands for the moment of inertia of core. V_0, the strength of the effective interaction both for particle-particle and particle-hole combination is assumed to be equal. In order to fit the AMR configuration, we set $J_{\pi_1} = J_{\pi_2} = J_\pi$ in what follows. The observed total angular momentum is obtained by minimizing energy w.r.t. θ in Eq. 2. This is mathematically given by $\frac{\partial E}{\partial \theta} = 0$. Imposing this condition, Eq. (2) simplifies to

$$I = (2J_\pi \cos\theta + J_\nu) + \frac{3I_m V_0}{J_\pi} \cos\theta (n_\pi n_\nu - 2n_\pi^2 \cos 2\theta) \quad (3)$$

Finally, with the help of the canonical relation $\omega = \frac{\partial E}{\partial \theta}$, ω is given by

$$\omega = \omega_0 + \frac{3V_0}{J_\pi} \cos\theta (n_\pi n_\nu - 2n_\pi^2 \cos 2\theta) \quad (4)$$

Besides reproducing the energies and the neutron alignments of the various isotopes of Cd, the model has also reproduced the level energies of ^{101}Pd very satisfactorily [34] . In a more recent work [14], the SCM model has been further improved by including a superposition of one- and three-neutron aligned configurations. This development is quite important as configuration of the band head is one-neutron and at high spin, neutron alignment occurs with the states having three neutron configuration. The interpolation between one- and three-neutron configurations is modeled using a step function

$$f(\theta) = \frac{1 - \tanh(\alpha(\theta - \theta_c))}{2} \quad (5)$$

The complete details of the model and some applications are given in Ref. [14].

In the framework of the above SCM model, the reduced transition probability, $B(E2)$, is given by [6, 7]

$$B(E2) = \frac{15}{32\pi}(eQ)^2_{\rm eff}\left[1-\left(\frac{I-J_\nu-R}{2J_\pi}\right)^2\right]^2 \quad (6)$$

This can also be written alternatively in terms of the dynamical variable, θ as

$$B(E2) = \frac{15}{32\pi}(eQ)^2_{\rm eff}\sin^4\theta \quad (7)$$

where $Q_{\rm eff}$ is the effective quadrupole moment of the core.

Using the configuration assigned above to the negative yrast sequence of ^{103}Pd, the various parameters used for SCM calculations are as follows: $J_\pi = 6\hbar$, $J_{\nu_1} = 5.5\hbar$ and $J_{\nu_2} = 11.5\hbar$. Further $n_{\nu_1} = 1$ and $n_{\nu_2} = 3$ as has been used in Ref. [14] for ^{101}Pd. Here the proton blades are formed through the participation of two proton-holes, each thus giving $n_\pi = 2$. The equations 3 and 4 were fitted to the experimental data and the parameters obtained in the fitting process are : $\omega_0 = 0.21\ MeV\hbar^{-1}$, $I_m = 13\ MeV^{-1}\hbar^2$ and $V_0 = 0.24\ MeV$, $\alpha = 25$ and $\theta_c^\circ = 57^\circ$. Although the parameters can be used to fit any given quantity, however, once the best fit is obtained for the level energies, the parameters are used to calculate the $B(E2)$ rates. The good agreement for $B(E2)$ rate provides an essential consistency check for the model calculations. Further, the parameters corresponding to the best fit are consistent with those obtained for other nuclei in this mass region [14]. The value of $eQ_{\rm eff}$ in the present calculations was taken as 1.22 eb. Its value in Ref. [16] was chosen as 1.3 eb. However, the quadrupole deformation of ^{103}Pd is slightly smaller than that of ^{104}Pd, which can be seen from Fig. 3 of Ref. [20], and hence the value of 1.22 eb was adopted.

The calculated quantities of angular momentum I, and $B(E2)$ obtained from the modified SCM approach are displayed in Figs. 5 and 6 respectively, along with the experimental and TAC-CDFT model approach. It is not surprising that SCM calculated I follows the experimental values as it has been fitted. It is interesting to note that the step function used to interpolate between one and three neutron configurations, nicely takes into account the change in the slope of the curve at about $\hbar\omega = 0.58$ MeV. It is evident from FIG. 6 that predicted $B(E2)$ from SCM approach reproduces the experimental data reasonably well, although the large value of $B(E2)$ for the first measured point is under-predicted. Besides, the $\Im^{(2)}/B(E2)$ values as seen from Table I above are large as expected for AMR bands. Thus, in the light of all the calculations in the framework of TAC-CDFT as well as SCM and the observation of large $\Im^{(2)}/B(E2)$ values, we can conclude that the negative parity yrast sequence of ^{103}Pd is a potential candidate that originates from the mechanism of antimagnetic rotation. The AMR motion involves the closing of two blades, each containing a proton-hole pair, to generate the high angular momentum states.

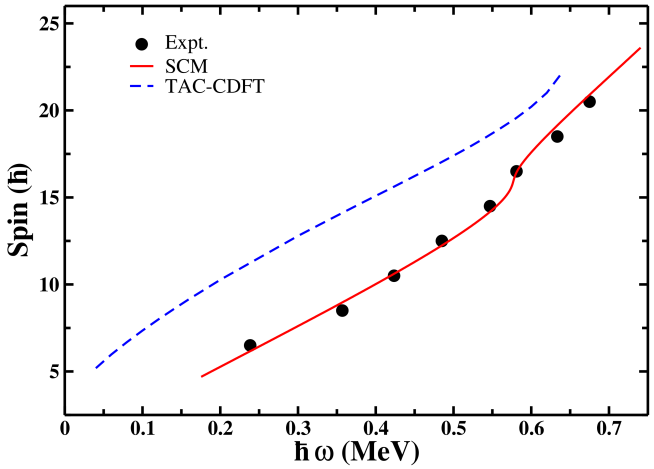

FIG. 5. The experimental values of spin versus rotational frequency are compared with those predicted by SCM and TAC-CDFT calculations.

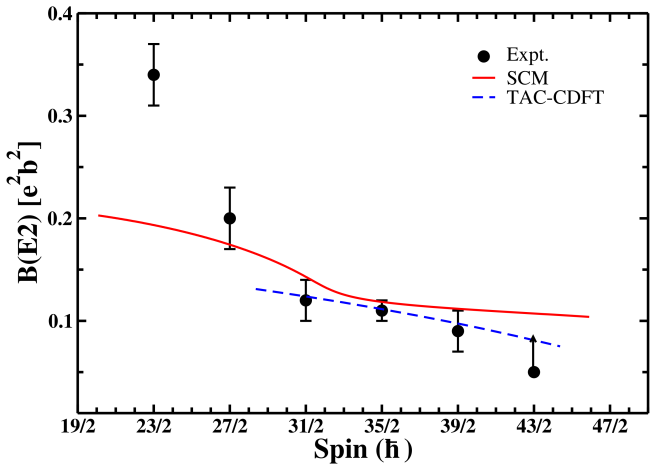

FIG. 6. Comparison of extracted $B(E2)$ rates versus spin for negative parity yrast band of ^{103}Pd with the SCM and TAC-CDFT model.

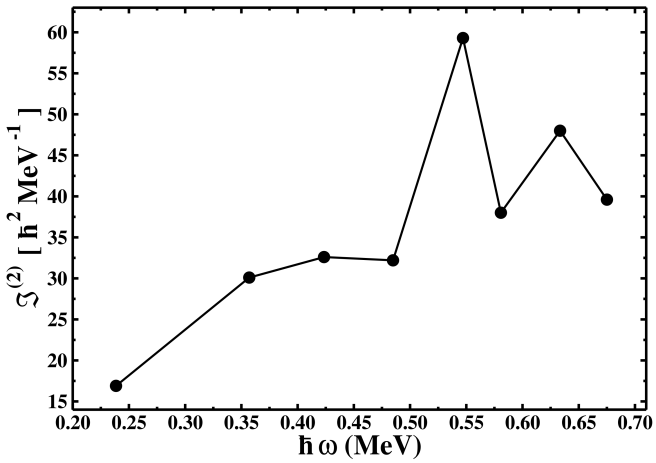

FIG. 7. The extracted dynamic moment of inertia as a function of rotational frequency from the experimental data.

We shall now turn our discussion to the band crossing features in the yrast sequence of ^{103}Pd. The nature of the band crossings in odd-Pd isotopes has been examined using different theoretical approaches with contradictory conclusions. In Refs. [14, 34], alignment of neutrons is assumed in the SCM to reproduce the experimental data for ^{101}Pd. However, it has been demonstrated using cranked Nilsson plus monopole pairing model with particle-number projection that first bandcrossing is due to the alignment of two protons [21]. In FIG. 7, $\Im^{(2)}$ evaluated from the experimental data is displayed as a function of rotational frequency and it clearly depicts two band crossings, one at $\hbar\omega \sim 0.55$ MeV and the other at about 0.64 MeV. In order to investigate the nature of the two band crossings, we have performed cranked shell model (CSM) calculations with Woods-Saxon potential and monopole pairing as used in the TRS study. The single quasi-particle routhians were calculated at deformation values of $(\beta_2, \gamma) = (0.16, 0°)$, which was determined from lifetime measurement of $I = 15/2^-$ state by Ashley *et al.* [38] and also predicted by TRS calculations at lower rotational frequencies. The routhians are plotted in FIG. 8 and it is evident from the figure that two-proton alignment occurs at $\hbar\omega = 0.48$ MeV and two neutron alignment in the positive parity states occurs at $\hbar\omega = 0.50$ MeV. The first bandcrossing in the negative parity states is blocked due to the odd-neuton occupying the $h_{11/2}$ orbital. This almost simultaneous crossing of protons and neutrons are in complete disagreement with the experimentally deduced band crossings.

As a matter of fact, it is not unexpected that band crossing frequencies are wrongly predicted by CSM as the deformation value used in the calculations is a factor of two lower than the measured values obtained in the present work. We have also performed CSM analysis using the deformation value of $\beta_2 = 0.34$, which is deduced from measured $B(E2)$ value at $I = 23/2^-$ state. The CSM single quasi-particle energies for this deformation value are displayed in the lower panel of FIG. 8. It is evident from this plot, that neutron BC-crossing (notation followed as given in Ref. [39]) occurs at about $\hbar\omega = 0.55$ MeV and the proton crossing crops up at about 0.63 MeV. These crossing features appear to be consistent with the peaks observed in the experimentally deduced $\Im^{(2)}$ of FIG. 7.

It is evident from the above CSM analysis that the calculated band crossings critically depend on the deformation value used in the CSM calculations. For smaller deformation values [40], the proton crossing occurs before the neutron crossing and further this neutron crossing is due to the alignment of two-neutrons in the N=4 shell. For large deformation values, neutron BC-crossing in the N=5 shell occurs before the proton crossing. The experimental data, obtained in the present work, clearly demonstrates that deformation changes with angular momentum along the yrast line and a fixed value of deformation cannot be employed in the CSM analysis. What is required is to perform a constrained self-consistent

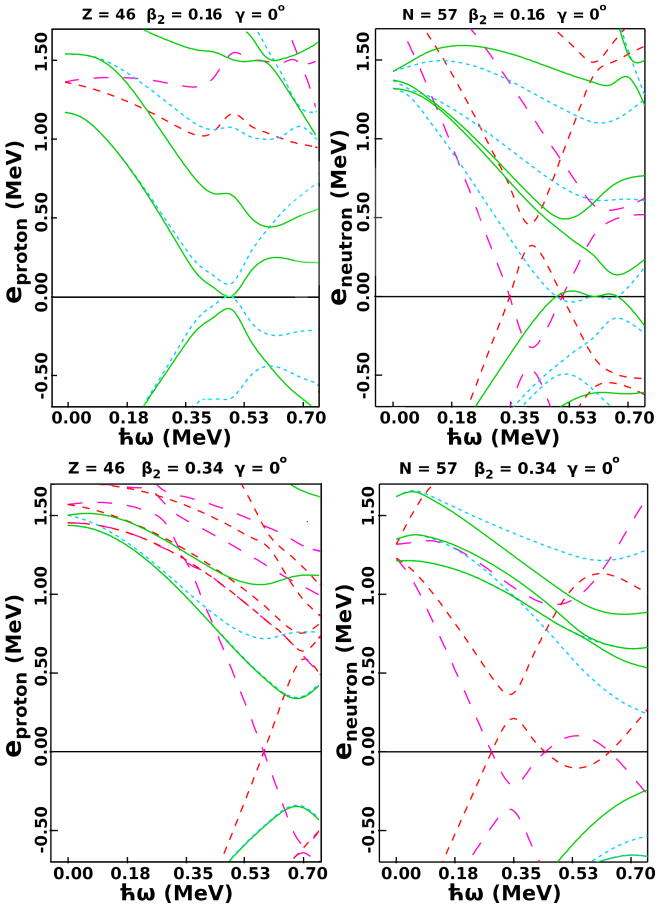

FIG. 8. The quasi-particle Routhians for proton and neutron calculated using cranked-shell model with the deformation parameters β_2= 0.16, $\gamma = 0°$ (Upper panel) and β_2= 0.34, $\gamma = 0°$ (Lower panel). Green and blue lines denote the positive parity, positive signature and positive parity, negative signature, respectively, whereas the red and magenta lines denote the negative parity, positive signature and the negative parity, negative signature respectively.

mean-field calculations with realistic effective interaction at each rotational frequency and evaluate the observable quantities. This work will unravel shape changes as a function of rotational frequency or angular momentum.

VI. CONCLUSION

Lifetime measurements, using the DSAM technique, have been carried out for the states of negative parity yrast band in ^{103}Pd nucleus. The trend of decreasing $B(E2)$ with increasing spin indicates that the band may be emerging from the AMR phenomenon. This is in conformity with the theoretical predictions within TAC-CDFT framework and the modified SCM analysis, and extends the list of observational evidence of such structures in this (A$\approx$ 100) region. Moreover, the agreement of the present experimental results with that of

the TAC-CDFT, as reported in Ref. [20], also suggest that the AMR sequence in ^{103}Pd can be interpreted to be emerging from alignment of four proton-hole blades with neutron-particle angular momentum vectors. The experimental results have also been satisfactorily reproduced in the calculations using the semi-classical particle rotor model, which has been successfully employed to investigate the AMR bands in this region. The modified SCM, which interpolates one- and three- neutron configurations with a step function is able to reproduce the up-bend observed in the angular momentum plot verses the rotational frequency. It has been further observed that TRS calculations significantly under-predict the measured $B(E2)$ values and what is required is to perform constrained mean-field study with realistic effective interaction to probe the shape changes along the yrast sequence of ^{103}Pd.

ACKNOWLEDGEMENT

The authors would like to thank the technical staff of IUAC pelletron facility for delivering stable beam during the experiment. We acknowledge the INGA Collaboration, UGC and DST for providing support under INGA project (IR/S2/PF-03/2003-I). We would also like to thank our colleagues Ritika Garg, Gurmeet Kumar, M. Idrees, Vishnu Jyoti and Indu Bala for their help during the experiment. Valuable suggestions and support received during analysis from Himanshu K. Singh (IIT, Bombay) and Sutanu Bhattacharya (GGV, Bilaspur) are highly appreciated. Discussions with Dr. B. Qi and Dr. H. Jia (Shandong University) of their TAC-CDFT results on AMR in this nucleus are gratefully acknowledged. A. Sharma is grateful to the Inter University Accelerator Centre, New Delhi for financial support *vide* UFR # 62316. U. Garg acknowledges the partial support by the U.S. National Science Foundation (Grant No. PHY-1419765 and PHY-1713857) for this work. R. Palit acknowledges the support from the Department of Atomic Energy, Government of India (Project Identification Code: 12-R&D-TFR-5.02-0200). Authors (GHB, NR and JAS) would like to acknowledge Department of Science and Technology, Govt. of India for providing financial support under Project no. CRG/2019/004960 to carry out a part of the research work. The author NR also acknowledges University Grant Commission for the Start-Up Grant No. F. 30-498/2019(BSR), dated 18-05-2019.

[1] A. Bohr and B. R. Mottelson, Nuclear Structure Vol. II, (Benjamin, New York, 1975).
[2] S. Frauendorf, Nuclear Physics A 557, 259 (1993).
[3] R. M. Clark and A. O. Macchiavelli, Annu. Rev. Nucl. Part. Sci. 50, 1 (2000).
[4] H. Hübel, Prog. Part. Nucl. Phys. 54, 1 (2005).
[5] S. Frauendorf, Rev. Mod. Phys. 73, 463 (2001).
[6] D. Choudhury, A. K. Jain, *et al.*, Phys. Rev. C 82, 061308 (2010).
[7] A. J. Simons, *et al.*, Phys. Rev. Lett. 91, 162501 (2003).
[8] D. Choudhury, A. K. Jain, *et al.*, Phys. Rev. C 87, 034304 (2013)
[9] A. J. Simons, R. Wadsworth, D. G. Jenkins, *et al.*, Phys. Rev. C 72, 024318 (2005).
[10] P. Datta, S. Chattopadhyay, S. Bhattacharya, *et al.*, Phys. Rev. C 71, 041305 (2005).
[11] C. J. Chiara, S. J. Asztalos, B. Busse, *et al.*, Phys. Rev. C 61, 034318 (2000).
[12] S. Roy, S. Chattopadhyay, P. Datta, *et al.*, Phys. Lett. B 694, 322 (2011).
[13] S. Zhu *et al.*, Phys. Rev. C 64, 041302 (2001).
[14] M. Sugawara *et al.*, Phys. Rev. C 92, 024309 (2015).
[15] V. Singh, S. Sihotra, *et al.*, J. Phys. G 44, 075105 (2017).
[16] N. Rather *et al.*, Phys. Rev. C 89, 061303 (2014).
[17] S. Silhotra *et al.*, Phys. Rev. C 102, 034321 (2020).
[18] D. Jerrestam, S. Mitarai, *et al.*, Nucl. Phys. A 557, 411 (1993).
[19] B. M. Nyak *et al.*, Phys. Rev. C 60, 024307 (1999).
[20] H. Jia, B. Qi, *et al.*, Phys. Rev. C 97, 024335 (2018).
[21] Z. H. Zhang *et al.*, Phys. Rev. C 94, 034305 (2016).
[22] A. O. Macchiavelli, *et al.*, Phys. Lett. B 450, 1 (1999).
[23] G. Mehta and A. Patro, Nucl. Instrum. Methods Phys. Res. Sect. A 268, 334 (1988).
[24] S. Muralithar, K. Rani, R. Kumar, R. P. Singh, *et al.*, Nucl. Instrum. Methods Phys. Res. Sect. A 622, 281 (2010).
[25] B. P. A. Kumar, E. T. Subramaniam, and R. K. Bhowmik, in Proc. DAE Symp. Nucl. Phys., Vol. 44B (2001) p. 390.
[26] R. Bhowmik, S. Muralithar, and R. P. Singh, in Proc. DAE Symp. Nucl. Phys., Vol. 44B (2001) p. 422.
[27] D. Radford, Nucl. Instrum. Methods Phys. Res. Sect. A 361, 297 (1995).
[28] J. C. Wells and N. R. Johnson, Report No. ORNL-6689, 44 (1991).
[29] S. Das, S. Samanta, R. Bhattacharjee, R. Raut, S. Ghugre, *et al.*, Nucl. Instrum. Methods Phys. Res. Sect. A 841, 17 (2017).
[30] www.srim.org,.
[31] A. Gavron, Phys. Rev. C 21, 230 (1980).
[32] C. S. Wu *et al.*, Phys. Rev. C 45, 261 (1992).
[33] R. Bhattacharjee, S. S. Bhattacharjee, *et al.*, Phys. Rev. C 90, 044319 (2014).
[34] M. Sugawara *et al.*, Phys. Rev. C 86, 034326 (2012).
[35] W. Nazarewicz, J. Dudek, R. Bengtsson, T. Bengtsson and I. Ragnarsson Nucl. Phys. A 435, 397 (1985).
[36] W. Nazarewicz, M.A. Riely, and J.D. Garrett, Nucl. Phys. A 512, 61 (1990).
[37] R. Wyss, J. Nyberg, *et al.*, Phys. Lett. B 215, 211 (1988).
[38] S. F. Ashley, P. H. Regan, K. Andgren, *et al.*, Phys. Rev. C 76, 064302 (2007).
[39] Tord Bengtsson, Nucl. Phys. A 512, 124 (1990).

[40] P. H. Regan, G. D. Dracoulis, *et al.*, J. Phys. G 19, L157 (1993).